The Astrophysical Journal, 682:767–774, 2008 August 1

POSSIBLE GeV EMISSION FROM TeV BLAZARS

C. Y. Yang, J. Fang, G. F. Lin, and L. Zhang
Department of Physics, Yunnan University, Kunming, China
Received 2008 January 17; accepted 2008 April 11

ABSTRACT

We propose a model to account for possible GeV emission from TeV blazars. In this model, the possible GeV emission from a TeV blazar can consist of two components. One, the source component, is produced in the source through the synchrotron self-Compton (SSC) mechanism; the other, the external component, is produced on the way from the source to us by the inverse Compton (IC) scattering of $e^{\pm}$ pairs with the cosmic microwave background (CMB), where the $e^{\pm}$ are created through the interaction of TeV gamma rays emitted from the TeV blazar with the diffuse IR-UV background. We apply the model to study the possible GeV emission from Mrk 501, which is a strong TeV emitter. We calculate self-consistently the spectra of high-energy gamma rays of these two components for three different activities of Mrk 501 in 1997. Our results indicate that (1) the GeV gamma-ray emission of the external component can dominate that of the source component if the intergalactic magnetic field (IGMF) strength is not greater than 10^{-19} G; (2) the shape of the photon spectra of the external component depends on both the observed variation time and the IGMF strength, particularly in the lower part of GeV energy range; (3) the flux level of TeV photons determines that of the spectrum of the external component; and (4) GeV emission from different activity in Mrk 501 should be detectable by the upcoming satellite *GLAST*.

Subject headings: BL Lacertae objects: general — BL Lacertae objects: individual (Mrk 501) — radiation mechanisms: nonthermal

1. INTRODUCTION

Observations of very high energy (VHE) gamma rays indicate that nearly 20 blazars emit gamma rays in the TeV energy region (e.g., Aharonian et al. 2005; Cui 2007; Wagner 2008). Almost all these blazars are BL Lacertae (BL Lac) objects. There are two kinds of models describing photon emission produced inside these TeV blazars: leptonic and hadronic models. In the leptonic models, nonthermal photon production mechanisms are believed to be synchrotron radiation and inverse Compton (IC) scattering by nonthermal particles in relativistically moving jets. Synchrotron self-Compton (SSC) models (e.g., Maraschi et al. 1992; Mastichiadis & Kirk 1997; Kino et al. 2002; Katarzynski et al. 2001) or external inverse Compton (EIC) models (e.g., Sikora et al. 1994), depending on different soft photon fields, are widely used to explain the observed multi–wave band emission from the blazars. Because the lack of strong emission lines for BL Lac objects is commonly taken as evidence that ambient fields are not important, the SSC models are more likely to explain the data than the EIC models (e.g., Krawczynski 2004). As to the hadronic models, high-energy gamma rays are produced by mesons and leptons through the cascade initiated by proton-proton or proton-photon interactions (e.g., Mannheim & Biermann 1992; Mannheim 1993; Mucke & Protheroe 2001).

It is believed that the TeV photons from the TeV blazars will interact with the IR-UV background to form electron-positron ($e^{\pm}$) pairs, leading to a significant fraction of them being absorbed (e.g., Nikishov 1962; Gould & Schréder 1966). After the discovery of extragalactic TeV gamma-ray sources, the effects of cosmological pair creation on their spectra were studied widely (e.g., Malkan & Stecker 1998; Konopelko et al. 1999; Primack et al. 1999; Hauser & Dwek 2001; Kneiske et al. 2002, 2004; Dwek & Krennrich 2005; Stecker et al. 2006). Observations of blazars in the TeV energy range can provide an ideal opportunity for determining the extragalactic background light intensity if their intrinsic spectral energy distribution (SED) is given (e.g., Dwek & Krennrich 2005), and different extragalactic background light (EBL) models have been proposed to construct self-consistent models of TeV blazars and the EBL spectrum. For example, Konopelko et al. (2003) solved kinetic equations of electrons and photons simultaneously to calculate the emission spectrum of Mrk 501 and Mrk 421, using the EBL models by Malkan & Stecker (2001) and de Jager & Stecker (2002) to calculate the optical depth for the TeV photons. Kato et al. (2006) set constraints on the physical condition of H1426+428 with the SSC model by applying several EBL models.

On the other hand, the $e^{\pm}$ pairs produced in the $\gamma + \gamma \longrightarrow e^{+} + e^{-}$ process may produce a new GeV emission component in TeV blazars through IC scattering of these $e^{\pm}$ pairs against cosmic microwave background (CMB) photons (Dai et al. 2002). For a blazar with an observed TeV spectrum, the $e^{\pm}$ spectrum can be estimated if the optical depth or intergalactic gamma-ray absorption coefficient is given. Dai et al. (2002) studied this new GeV emission from TeV blazars and estimated the scattered photon flux of Mrk 501, using the intrinsic TeV spectra of Mrk 501 during its 1997 high state taken from de Jager & Stecker (2002). They predicted strong GeV emission produced by this process for Mrk 501 when the intergalactic magnetic field (IGMF) is weak enough. Following Dai et al. (2002), Fan et al. (2004) studied the blazar H1426+428 with a relatively high redshift $z = 0.129$. They numerically calculated the scattered photon spectra for different IGMF strengths and predicted very strong GeV emission with flux far above the detection sensitivity of the upcoming satellite *GLAST* (*Gamma-Ray Large Area Space Telescope*) if the IGMF is about 10^{-18} G or weaker.

In this paper, we make a self-consistent study of the possible origin of GeV emission from Mrk 501. The GeV emission from TeV blazars consists of two components: one, the source component, comes from the source; and the other, the external component, comes from IC scattering of high-energy pairs produced through pair-production process of TeV photons and the IR-UV background against the CMB photons. We use the SSC model

given by Mastichiadis & Kirk (1997) to calculate the nonthermal photon spectrum of the source component for a given TeV blazar. For the external component, unlike Dai et al. (2002) and Fan et al. (2004), we use the predicted results, which fit the observed data very well, within the frame of the SSC model to derive the intrinsic photon spectrum by using recent models for the optical depth, estimate the spectrum of high-energy pairs, and then calculate the nonthermal photon spectrum of the external component. We use two kinds of models for the optical depth in our calculations: one is the analytic approximation for the optical depth given by Stecker et al. (2006, 2007), and the other is given by Kneiske et al. (2004), in which the optical depth is calculated based on a semiempirical model for the EBL. The paper is organized as follows: We describe the model briefly in § 2. In § 3, we apply the model to Mrk 501, and finally we give our conclusion and discussion in § 4.

2. THE MODEL

We now describe the model for possible GeV emission from a TeV blazar that is observable from the Earth. As mentioned in § 1, the GeV emission consists of source and external components. We calculate the nonthermal photon spectra of the source component within the frame of SSC model and those of the external component by using the method given by Fan et al. (2004). We now briefly describe the production processes.

2.1. *Nonthermal Photons Produced in the Source*

For the nonthermal photons produced in TeV blazars, we adopt the SSC model described in Mastichiadis & Kirk (1997). In this model, it is assumed that a single homogeneous emission region both emits synchrotron photons directly and scatters them to high (gamma-ray) energy before emission (i.e., SSC model), and full time-dependent evolution of the electron and photon spectra are followed by assuming a power-law form of the electron injection, i.e., $Q_e = q_e\gamma^{-s}\exp(-\gamma/\gamma_{\max})$ for $\gamma_{\min} \le \gamma \le \gamma_{\max}$, where γ is the electron Lorentz factor, s is the spectral index, and $\gamma_{\min}$ and $\gamma_{\max}$ are the minimum and maximum electron Lorentz factors, respectively.

The equations governing the evolution of the electron distribution n_e and photon distribution n_γ are given by Mastichiadis & Kirk (1997):

$$\frac{\partial n_e(\gamma,t)}{\partial t} + \frac{n_e(\gamma,t)}{t_{\rm esc}} = Q_e\left(n_e,n_\gamma,\gamma,t\right) + L_e\left(n_e,n_\gamma,\gamma,t\right), \quad (1)$$

$$\frac{\partial n_\gamma(x,t)}{\partial t} + \frac{n_\gamma(x,t)}{t_{\gamma,\rm esc}} = Q_\gamma\left(n_\gamma,n_e,x,t\right) + L_\gamma\left(n_\gamma,n_e,x,t\right), \quad (2)$$

respectively, where $t_{\rm esc}$ is average residence time of electrons, L_e describes the electron loss terms, $x = h\nu/(m_ec^2)$ is the dimensionless photon frequency, $t_{\gamma,\rm esc}$ is the time that photons leave the source in units of the light crossing time $t_{\rm cross} = R/c$ (where R is source radius), Q_γ represents photon source terms, and L_γ is the photon loss term. The details of the above equations are described in Mastichiadis & Kirk (1995, 1997); here we neglect them.

In this model, once the injection function for relativistic electrons is given, the two time-dependent kinetic equations for the electron and photon distributions are solved. The parameters include the Doppler factor δ, source radius R, magnetic field strength B, electron spectral index s, electron maximum Lorentz factor $\gamma_{\max}$, electron injection compactness $l_e = \frac{1}{3}m_ec\sigma_{\rm T}R^2\int_1^\infty d\gamma\,(d\gamma-1)Q_e$, and effective escape time $t_{\rm esc}$. Mastichiadis & Kirk (1997) used their model to account for the multiwavelength spectra of Mrk 421 during quiescent and flaring states. Their method was to find detailed fits to the quiescent spectrum at first, and then to explain the flaring activity by changing the electron parameters q_e and/or $\gamma_{\max}$ or by changing the magnetic field. In other words, the full time-dependent behavior of flares was obtained by fitting the quiescent spectrum of the source and then varying one of the free parameters. Mastichiadis & Kirk (1997) have shown that the time dependence of the keV/TeV flare could be the result of a sudden increase in the maximum energy of the injected electrons.

Following the method of Mastichiadis & Kirk (1997), we can numerically calculate equations (1) and (2) using reasonable parameters and obtain the nonthermal photon spectrum for a given TeV blazar (e.g., Mrk 501). In other words, the intrinsic photon spectrum, $dN_\gamma^{\rm int}/dE_\gamma$, for a TeV blazar is given by calculating equations (1) and (2). Furthermore, a significant fraction of photons will be absorbed when high-energy photons propagate through the extragalactic background light field. If $\tau(E'_\gamma,z)$ is the optical depth due to the absorption of extragalactic background light, where z is the redshift, $E'_\gamma \equiv (1+z)E_\gamma$ is the photon energy in the local frame, and E_γ is the observed energy, then the observed spectrum is given by

$$\frac{dN_\gamma^{\rm obs}}{dE'_\gamma} = \frac{dN_\gamma^{\rm int}}{dE'_\gamma}\exp\left[-\tau\left(E'_\gamma,z\right)\right]. \quad (3)$$

We use equation (3) to fit the observed data of a given TeV blazar. From equation (3), we can see that an important quantity in deriving the observed photon spectrum is the optical depth or intergalactic gamma-ray absorption coefficient, $\tau(E'_\gamma,z)$, which is a function of the redshift z for a given energy.

Various models for the optical depth $\tau(E'_\gamma,z)$ have been proposed (e.g., Stecker et al. 1992, 1996, 2006, 2007; Stecker & de Jager 1998; Primack et al. 1999; de Jager & Stecker 2002; Kneiske et al. 2004; Dwek & Krennrich 2005). Here we use two kinds of models for the optical depth to calculate $\tau(E'_\gamma,z)$. One is the analytic fit with numerical coefficients for the approximation of the optical depth given by Stecker et al. (2006, 2007) for gamma rays having energies from 4 GeV to 100 TeV emitted by sources at redshifts from 0 to 5. The analytic approximation is (Stecker et al. 2006)

$$\log\tau\left(E'_\gamma,z\right) = Ax^4 + Bx^3 + Cx^2 + Dx + E, \quad (4)$$

where $x = \log E'_\gamma(\rm eV)$, and the coefficients A through E depend on the redshift and have been given in Table 1 in Stecker et al. (2006; see also Stecker et al. 2007). Equation (4) can be used over the range $0.01 < \tau < 100$. The other is the model given by Kneiske et al. (2004), in which the optical depth for a given TeV blazar can be calculated based on the model for the time-dependent EBL, where the redshift evolution of the EBL has been included (for the details of this model see Kneiske et al. 2004). As an example, we show the comparison of the change of the optical depth with photon energy in both models for redshift $z = 0.03$ (corresponding to the redshift value of Mrk 501) in Figure 1, where the solid line represents the optical depth by using Stecker et al. (2006), and the dash-dotted, dashed, and dotted lines denote the upper, averaged, and lower values of the optical depth given by Kneiske et al. (2004), respectively. It can be seen that the range bounded by the model of Kneiske et al. (2004) contains the main

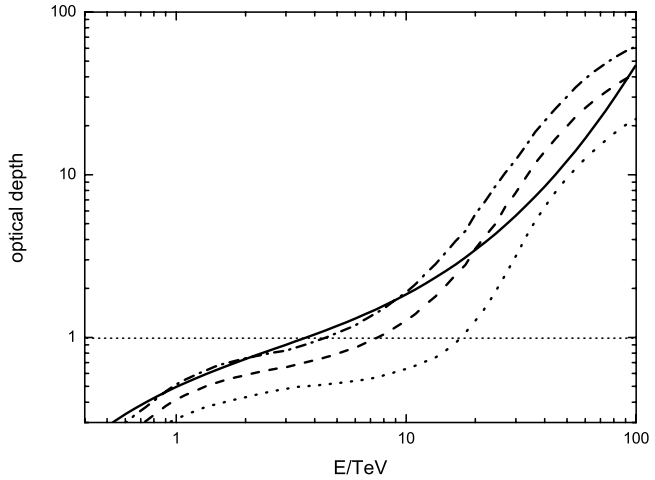

FIG. 1.—Optical depth at redshift $z = 0.03$. The solid line represents the optical depth calculated using the approximation given by Stecker et al. (2006). The dash-dotted, dashed, and dotted lines denote the upper, averaged, and lower values of optical depth given by Kneiske et al. (2004), respectively.

part of the result of Stecker et al. (2006), although the variations of the optical depth with photon energy in both models are different.

2.2. *Nonthermal Photons Produced Outside the Source*

As mentioned in § 2.1, since the interaction of high-energy photons with low-energy photons will produce electron/positron pairs, a significant fraction of very high energy (VHE) photons from a distant object will be absorbed when they propagate from the object to us. Following Dai et al. (2002) and Fan et al. (2004), we describe the model of GeV emission of TeV blazars. In this model, the main physical inputs include (1) an estimate of how many electron/positron pairs will be produced, (2) the intergalactic magnetic field (IGMF), and (3) the CMB photon field. In other words, using inputs 1, 2, and 3, we can estimate the possible GeV emission by inverse Compton scattering of the high-energy pairs off the CMB photon field. We now describe these processes.

According to equations (1)–(3), we can estimate absorbed VHE photon spectrum, $dN_\gamma^{\rm abs}/dE'_\gamma = dN_\gamma^{\rm int}/dE'_\gamma - dN_\gamma^{\rm obs}/dE'_\gamma$. The absorbed VHE photons will become high-energy electron/positron pairs. We assume that $dN_e/d\gamma_e$ is the spectrum of high-energy electrons with a Lorentz factor $\gamma_e \approx E'_\gamma/(2m_ec^2)$, where m_e is electron mass and c is the light speed. Therefore, using $E'_\gamma dN_\gamma^{\rm abs}/dE'_\gamma = \frac{1}{2}\gamma_e dN_e/d\gamma_e$, we have

$$\frac{dN_e}{d\gamma_e} = 2\times10^{-6}\frac{dN_\gamma^{\rm int}}{dE'_\gamma}\left\{1-\exp\left[-\tau\left(E'_\gamma,z\right)\right]\right\}. \quad (5)$$

These high-energy $e^\pm$ pairs will emit high-energy photons through inverse Compton scattering off the ambient CMB photons. Assuming the mean energy of the CMB photons is $\bar{\epsilon} = 2.7kT$ with $T \approx 2.73(1+z)$ K, where k is the Boltzmann constant, we have an average value of the boosting energy through the IC process of $\bar{E}_\gamma \sim \gamma_e^2\bar{\epsilon} \approx 0.63(1+z)(E_\gamma/1\ {\rm TeV})^2$ (Fan et al. 2004).

We now consider the minimum ($\gamma_{e,\min}$) and maximum ($\gamma_{e,\max}$) values of the high-energy $e^\pm$ pairs, i.e., the energy regime where equation (5) is available. As to the minimum value of Lorentz factor of high-energy electrons, generally $\gamma_{e,\min} \geq 1$. As pointed out by Fan et al. (2004; see also Dai et al. 2002), however, there is a lower limit on the Lorentz factor of high-energy electrons, $\gamma_{e,c}$: the photons produced by high-energy electrons with $\gamma_e < \gamma_{e,c}$ contribute little to GeV emission considered here. The estimate of $\gamma_{e,c}$ depends on GeV photon durations. There are four timescales involved in the GeV emission process: (1) the observed variability time of the source emission, $t_{\rm var,obs}$; (2) the well-known angular spreading time, $\Delta t_{A,\rm obs} \approx 960(1+z)(\gamma_e/10^6)^{-2}(n_{\rm IR}/0.1\ {\rm cm}^{-3})$, where $n_{\rm IR} \simeq 0.1\ {\rm cm}^{-3}$ is the intergalactic infrared photon number density (e.g., Dai & Lu 2002); (3) the IC cooling time, $\Delta t_{\rm IC,obs}$, which is approximated as $\Delta t_{\rm IC,obs} \approx 38(1+z)^{-3}(\gamma_e/10^6)^{-3}$ s (e.g., Fan et al. 2004); and (4) the magnetic deflection time, $\Delta t_{B,\rm obs} \approx 6.1\times10^3(\gamma_e/10^6)^{-5}(B_{\rm IG}/10^{-20}\ {\rm G})^2(1+z)^{-11}$ s (Plaga 1995; Dai et al. 2002; Fan et al. 2004), where $B_{\rm IG}$ is the intergalactic magnetic field in units of gauss. Following Fan et al. (2004), the duration estimate of the IC emission from electron/positron pairs scattering off the CMB is

$$\Delta t = \max\left(\Delta t_{\rm IC,obs}, \Delta t_{A,\rm obs}, \Delta t_{B,\rm obs}, t_{\rm var,obs}\right). \quad (6)$$

They argued that the typical duration of GeV emission is estimated by the source activity time and the energy-dependent magnetic deflection time, and introduced the critical Lorentz factor $\gamma_{e,c}$ by putting $\delta t_{A,\rm obs} = t_{\rm var,obs}$, which is (Fan et al. 2004)

$$\gamma_{e,c} \approx 5.9\times10^6\left(\frac{t_{\rm var,obs}}{1\ {\rm day}}\right)^{-1/5}\left(\frac{B_{\rm IG}}{10^{-20}\ {\rm G}}\right)^{2/5}(1+z)^{-11/5}. \quad (7)$$

We now consider the initial Lorentz factor of the electrons. We have $\gamma_e \approx E'_\gamma/(2m_ec^2)$, but this is only valid at the beginning because γ_e decrease with t, so we let $\gamma_{e,0} = E'_\gamma/(2m_ec^2)$, and electron energy loss rate by the IC scatter with CMB photons in propagation is $dE_e/dt = b\gamma_e^2$ with $b = \frac{4}{3}\sigma_{\rm T}U_{\rm CMB}c$, where $U_{\rm CMB}$ is background photon energy density, $\sigma_{\rm T}$ is Thomson cross section, and c is the light speed. Therefore, the electron Lorentz factor changing with time is given by

$$\gamma_e(t) = \gamma_{e,0}\frac{1}{1+b\gamma_{e,0}}, \quad (8)$$

and $\gamma_{e,\max}$ is assumed to be the initial electron maximum Lorentz factor according to $\gamma_{e,\max} = E'_{\gamma,\max}/(2m_ec^2)$, which also changes with t just as equation (8), where $E'_{\gamma,\max}$ is the maximum emissive energy in the blob. For the electrons, $\gamma_{e,c} < \gamma_e(t) \leq \gamma_{e,\max}(t)$; therefore, the magnetic deflection angle is so small that most of the scattered CMB photons that contribute to GeV emission can reach the observer in finite time $t_{\rm var,obs}$.

After determining the spectrum of high-energy electrons that satisfies equation (5) with $\gamma_{e,c} < \gamma_e(t) \leq \gamma_{e,\max}(t)$, the time-averaged scattered photon spectrum through the IC process is given by (e.g., Blumenthal & Gould 1970; Dai et al. 2002; Fan et al. 2004)

$$\frac{dN_\gamma^{\rm IC}}{dE_\gamma} = \frac{1}{4\pi D_L^2}\int\int\int\left(\frac{dN_e}{d\gamma_e}\right)\frac{n(\epsilon)\,d\epsilon}{\epsilon^2}F\left(E_\gamma,\gamma_e,\epsilon\right)dt\,d\gamma_e, \quad (9)$$

where E_γ is the externally scattered photon energy, D_L is the luminosity distance to the source, t is the time measured in the local rest frame, and $n(\epsilon)\,d\epsilon$ is the differential number density of the CMB photons, which is approximated by a blackbody law,

$$n(\epsilon) = \left[\pi^2(\hbar c)^3\right]^{-1}\frac{\epsilon^2}{e^{\epsilon/kT}-1}. \quad (10)$$

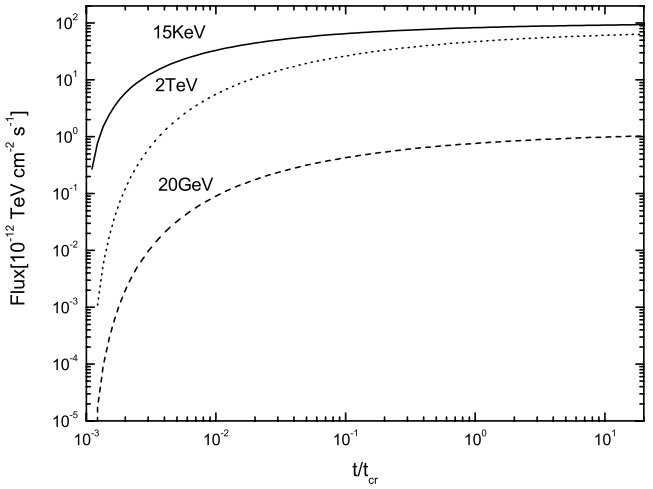

FIG. 2.—Evolution of the spectra at three energies, 15 keV (*solid line*), 20 GeV (*dashed line*), and 2 TeV (*dotted line*), with time for the LF of Mrk 501. The model parameters are listed in Table 1.

The function $F(E_\gamma, \gamma_e, \epsilon)$ is given by

$$F(E_\gamma, \gamma_e, \epsilon) = \frac{\pi r_0^2 c}{2\gamma_e^4}\left[2E_\gamma \ln\left(\frac{E_\gamma}{4\gamma_e^2\epsilon}\right) + E_\gamma + 4\gamma_e^2\epsilon - \frac{E_\gamma^2}{2\gamma_e^2\epsilon}\right], \quad (11)$$

where r_0 is the electron classical radius. In equation (9), following Fan et al. (2004), the integration for the variable t ranges from 0 to $7.7\times10^{13}(1+z)^{-4}(\gamma_{e,c}/10^6)^{-1}$ s, and the integration for the variable $\gamma_e(t)$ ranges from $\gamma_{e,c}$ to $\gamma_{e,\max}(t)$.

We use $(dN/dE)_{\rm source}$ to denote the nonthermal spectrum of photons produced in the source by the SSC model [i.e., the source component, $(dN/dE)_{\rm source} = (dN_\gamma^{\rm obs}/dE_\gamma)$] and $(dN/dE)_{\rm ex}$ to represent the spectrum of photons produced outside the source through IC scattering of high-energy pairs produced through pair-production process of TeV photons and the IR-UV background against the CMB photons [i.e., the external component, $(dN/dE)_{\rm ex} = (dN_\gamma^{\rm IC}/dE_\gamma)$]. Therefore, the photon spectrum that is observable from the Earth is given by

$$\frac{dN}{dE} = \left(\frac{dN}{dE}\right)_{\rm source} + \left(\frac{dN}{dE}\right)_{\rm ex}. \quad (12)$$

3. APPLICATION TO MRK 501

We now apply the model to Mrk 501, an extragalactic TeV gamma-ray source with rapid variations and a redshift of $z = 0.034$. It was discovered at the TeV energy range by the Whipple Observatory (Quinn et al. 1996) and confirmed by HEGRA (Bradbury et al. 1997). Djannati-Atai et al. (1999) reported VHE gamma-ray spectral properties of Mrk 501 from CAT observations in 1997. Since the TeV emission from Mrk 501 was discovered, observations in different energy ranges have been performed and long-term X-ray and TeV variability of Mrk 501 have been observed (e.g., Gliozzi et al. 2006). Here we use the data of VHE gamma-ray spectra given by Djannati-Atai et al. (1999), because of simultaneous and quasi-simultaneous observations of CAT VHE gamma rays and *BeppoSAX* hard X-rays during 1997.

In the spectral analysis of Djannati-Atai et al. (1999), the data set was taken from 1997 March to October, and three different activities of Mrk 501 were defined: a high-intensity flare (HF) with integral flux $\geq 50\times10^{-11}$ cm^{-2} s^{-1}, a low-intensity flare (LF) with integral flux $\leq 12\times10^{-11}$ cm^{-2} s^{-1}, and a midintensity flare (MF) with integral flux between those of the HF and the LF. In this paper, we consider these cases.

As an example, we show in Figure 2 the evolution of the spectra with time at three energies of 15 keV, 20 GeV, and 2 TeV for the LF of Mrk 501, with the parameters listed in Table 1. From Figure 2, the spectrum in the stationary state is obtained at roughly several $t_{\rm cross}$. Therefore, we can use the method of Mastichiadis & Kirk (1997) to describe the cases considered here.

We now apply the model described in § 2 to calculate the nonthermal spectra of Mrk 501 in the GeV energy range. According to this model, the emission in the GeV energy range for a given flare of Mrk 501 consists of source and external components. Our procedure for self-consistently calculating the nonthermal photon spectrum of these two components is as follows. First, we calculate the spectrum of the nonthermal photons produced in the source using the SSC model given by Mastichiadis & Kirk (1997; i.e., the source component). By solving equations (1) and (2) with suitable model parameters, we can obtain the intrinsic photon spectrum, and then the observed photon spectrum by using equation (3). We use equation (3) to fit the observed data in the X-ray and TeV energy bands by adjusting the model parameters. Therefore, we obtain the spectrum produced inside the source. Finally, we calculate the nonthermal photon spectrum produced outside the source (i.e., the external component). In order to do so, we estimate the electron/positron spectrum produced outside the source using equation (5), and then the photon spectrum using equation (9). We obtain the photon spectrum that is observable from the Earth using equation (12).

The predicted nonthermal spectra of the source component for the HF, the LF, and the MF of Mrk 501 are shown in Figure 3, where we fit the predicted results with the observed data in both X-ray and VHE gamma-ray bands and give the intrinsic spectra using the approximation for the optical depth given by Stecker et al. (2006). The model parameters of the best fits of the predicted results with the observed data are listed in Table 1, where the χ^2 values correspond to the fits of the model results with the observed

TABLE 1
PARAMETERS IN THE SSC MODEL USING THE STECKER ET AL. MODEL FOR THE OPTICAL DEPTH

State	δ	R (cm)	s	$\gamma_{\max}$	l_e	B (G)	$t_{\rm cross}/t_{\rm esc}$	χ^2/dof
HF	20	2.5×10^{16}	1.57	9×10^5	3.5×10^{-5}	0.1	1	0.79
MF.....	20	2.5×10^{16}	1.85	7×10^5	1.4×10^{-5}	0.1	1	1.57
LF.....	20	2.5×10^{16}	1.95	6×10^5	1.4×10^{-5}	0.1	1	1.47

NOTES.—The parameters in the SSC model are given by Mastichiadis & Kirk (1997) for reproducing the observed spectra in the HF, MF, and LF of Mrk 501 (Djannati-Atai et al. 1999). The analytic approximation for the optical depth given by Stecker et al. (2006, 2007) is used.

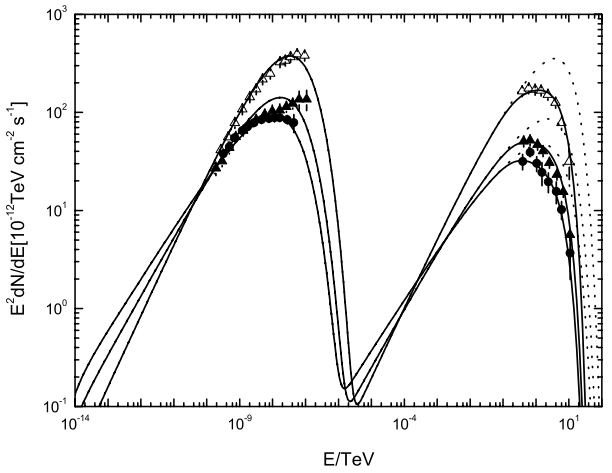

FIG. 3.—Comparison of predicted multiband spectra with the observed data in both X-ray and TeV energy ranges in the HF, MF, and LF of Mrk 501. Solid and dashed curves represent fitting spectra and intrinsic spectra, respectively, where the optical depth is calculated by using the formulae of Stecker et al. (2006). The parameters of the SSC model are listed in Table 1. The observed data for the HF (*open triangles*), MF (*filled triangles*), and LF (*filled circles*) are taken from Djannati-Atai et al. (1999).

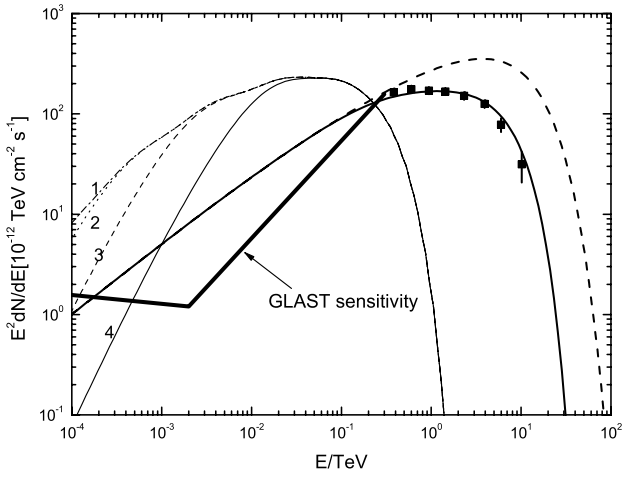

FIG. 4.—Time-averaged high-energy gamma-ray spectra of Mrk 501 for the high-intensity flare with $t_{\rm var,obs} = 0.5$ days. The thick solid and dashed curves represent the fitting and intrinsic spectra given by the SSC model, respectively (i.e., the spectra produced inside the source); curves 1–4 represent the secondary photon spectra produced by the resulting $e^{\pm}$ pairs interacting with CMB photons and correspond to IGMF strength of 10^{-22}, 10^{-20}, 10^{-19}, and 10^{-18} G, respectively (i.e., spectra produced outside the source). The filled squares represent the data by CAT (Djannati-Atai et al. 1999). The broken line is the *GLAST* sensitivity with integral time of 12 hr.

data in these three cases. From Table 1 and the relation between the observed minimum variation timescale $t_{\rm var,obs}$ and the radius of the source R, i.e., $t_{\rm var,obs} = R/(\delta c)$, we have $t_{\rm var,obs} \approx 0.5$ days. From Figure 3, it can be seen that this SSC model can reproduce the observed data well. In other words, the simultaneous observation of the spectral properties in both the X-ray and the VHE energy range is naturally expected in the SSC model.

Furthermore, we calculate the photon spectra of the external component (i.e., the spectra through the IC scattering of the resulting $e^{\pm}$ pairs against the CMB photons) for the three flares of Mrk 501. In our calculations for the emission of the external component, there are three important physical quantities: the electron spectrum $dN_e/d\gamma_e$, the observed variation time $t_{\rm var,obs}$, and the intergalactic magnetic field (IGMF) $B_{\rm IG}$. The shape and magnitude of the electron spectrum depends on those of TeV photons for a given flare of Mrk 501 (see eq. [5]). It should be pointed out that the estimate of the electron/positron spectrum and the value of $t_{\rm var,obs}$ used here are determined by the best fits of the emission of the source component to the observed data; therefore, our calculations are self-consistent. From equation (7), we note that $\gamma_{e,c}$ depends on both $t_{\rm var,obs}$ and $B_{\rm IG}$. The IGMF is an important physical quantity but has not been determined so far. For this object, it has been suggested that $B_{\rm IG} \leq 10^{-18}$ G (Aharonian et al. 2002). Theoretically, the IGMF would be of the order of 10^{-20} G or even as low as 10^{-29} G (see, e.g., Sigl et al. 1997; Fan et al. 2004). Therefore, we use the IGMF as a parameter ranging from 10^{-18} to 10^{-22} G in our calculations. In each active state, the spectra of the external component for different intergalactic magnetic fields are calculated, where the observed variation time is fixed to be 0.5 days.

In Figure 4, we show the best-fit and intrinsic spectra of the source component (also see Fig. 3), the predicted photon spectra of the external component for $B_{\rm IG} = 10^{-22}$, 10^{-20}, 10^{-19}, and 10^{-18} G, the observed data in TeV energy band for the HF of Mrk 501, and the sensitivity of *GLAST* with integral time of 12 hr. It can be seen from Figure 4 that the predicted photon spectrum of the external component depends on the value of the IGMF, and the contribution of the external component compared to that of the source component decreases as the IGMF increases, particularly in the lower energy range. In fact the predicted photon spectra of the external component for $B_{\rm IG} \leq 10^{-19}$ G dominates over those of the source component in the energy range of $E \lesssim 200$ GeV; however, the contribution of the component in the energy $E \leq 1$ GeV will become less important compared to the source component when $B_{\rm IG} = 10^{-18}$ G. From Figure 4, the photons in the energy range of 100 MeV $\leq E \lesssim 200$ GeV are mainly produced by the emission of the external component for $B_{\rm IG} \leq 10^{-19}$ G if *GLAST* can detect the GeV emission from Mrk 501 that is in the HF.

As mentioned above, the shape and the magnitude of the nonthermal photons of the external component depend on those of the electron spectrum, which is determined by the TeV photon spectrum for a given active state of Mrk 501. Therefore, we calculate the photon spectra of both the source and external components for the MF and the LF of Mrk 501; the results are shown in Figures 5 and 6, respectively. For the MF and the LF of Mrk 501, the GeV emission of the external component has the same properties as those of the HF. The main difference is the GeV flux levels, which decrease as the intensity of the flare decreases. This feature can influence the relative importance of GeV emission of the external component compared to the emission of the source component and the detection by *GLAST*. In fact, in the case of the MF of Mrk 501, the flux level in the GeV energy range is less than that for the HF of Mrk 501 (peak flux is $\sim 4 \times 10^{-11}$ TeV cm^{-2} s^{-1} for the MF, compared to the peak flux of $\sim 2 \times 10^{-10}$ TeV cm^{-2} s^{-1} for the HF; see Figs. 4 and 5). From Figure 5, the fluxes of the external component for $B_{\rm IG} \geq 10^{-20}$ G dominate over those of the source component in the energy range of 100 MeV $\leq E \lesssim 100$ GeV, but the flux of the external component for $B_{\rm IG} = 10^{-18}$ G is less than that of the source component in the energy range $E \lesssim 4$ GeV. Moreover *GLAST* will detect photon emission in this energy range, which comes mainly from the emission of the source component (see Fig. 5). For the case of the LF of Mrk 501, the features indicated in the case of the MF are more prominent. The predicted fluxes of

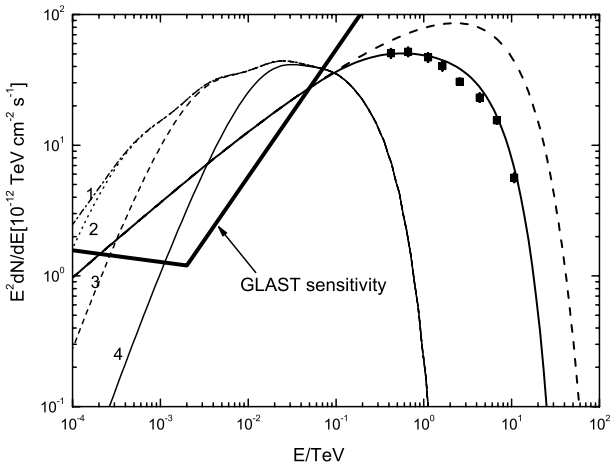

FIG. 5.—Same as Fig. 4, but for the midintensity flare.

the external and source components for the LF are shown in Figure 6 for the parameter ranges of $B_{\rm IG} = 10^{-18}$, 10^{-19}, 10^{-20}, and 10^{-20} G and $t_{\rm var,obs} = 0.5$ days. Compared to the case of the HF, the peak flux of the external component is less than that for the HF by a factor of $\sim$10. It can be seen from this figure that the GeV emission of the external component dominates over that of the source component only if $B_{\rm IG} \leq 10^{-19}$, but becomes less important if $B_{\rm IG} \geq 10^{-18}$ G, and the emission detectable by *GLAST* comes mainly from the source component.

It is clear that the contribution of the external component to GeV emission depends on the optical depth to high-energy photons. Therefore, it is necessary to use another model for the optical depth to check the above predicted results. Here we use the model given by Kneiske et al. (2004), and the changes of the optical depth with photon energy for Mrk 501 ($z = 0.03$) are shown in Figure 1. Following the calculation procedure described above, we fit the model results to the observed data in both X-ray and VHE gamma-ray bands for the HF, the LF, and the MF of Mrk 501 and obtain the corresponding intrinsic spectra. The results are shown in Figure 7 and the model parameters of the best fits are listed in Table 2, where the averaged value of the optical depth is used (Fig. 1, *dashed line*). It can be seen that the model parameters are different for two different models of the optical depth (see Tables 1 and 2). Moreover, the model spectra can reproduce the observed data of Mrk 501 well within the uncertainty of the optical depth given by Kneiske et al. (2004). We also note that the model result can reproduce the observed data of the LF of Mrk 501 very well (see Fig. 7 and Table 2); therefore, we consider this case as an example to account for the difference of the predicted GeV emission of the external component between these two different models for the optical depth. In Figure 8, we show the comparison of the model results of the external component in these two models for the optical depth for the LF of Mrk 501, where the parameters of the SSC model are listed in Table 2 and the IGMF strength of 10^{-22} G is used. For the intrinsic spectrum, which is estimated for the averaged value of the optical depth given by Kneiske et al. (2004), we calculate the observed spectra for upper, averaged, and lower values of the optical depth (see Fig. 8, *dashed, solid, and dash-dotted lines*) and the corresponding photon spectra of the external component. For comparison, in Figure 8 we also show the corresponding spectra (*dash–double-dotted lines*) for the optical depth given by Stecker et al. (2006), which are within the uncertainty of the model results for the optical depth given by Kneiske et al. (2004) and very close to those for the upper value of the optical depth. Although these two models for the optical depth used in this paper can result in different nonthermal photon spectra of the external component, our conclusions on the contribution of the external component to the GeV emission made by using the optical depth given by Stecker et al. (2006) are roughly unchanged.

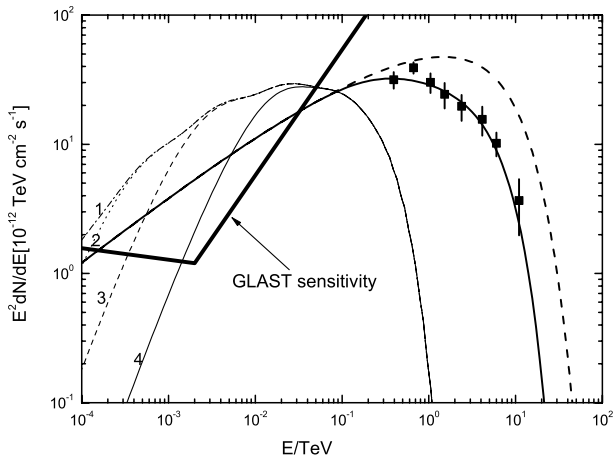

FIG. 6.—Same as Fig. 4, but for the low-intensity flare.

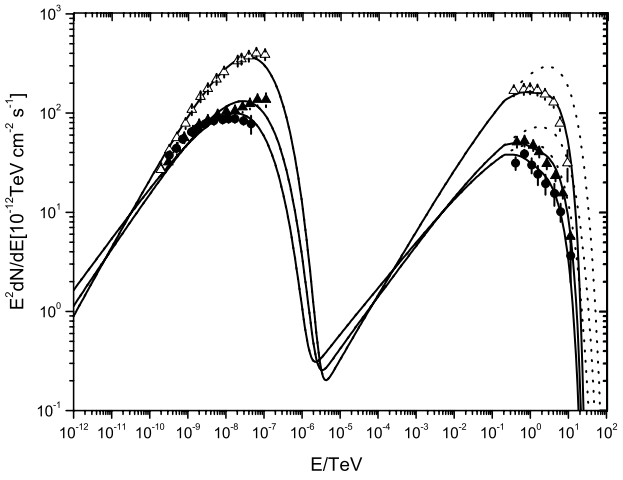

FIG. 7.—Comparison of predicted multiband spectra with the observed data in both X-ray and TeV energy ranges in the HF, MF, and LF of Mrk 501. Solid and dotted curves represent fitting spectra and intrinsic spectra, respectively, where the optical depth is calculated by using the average of both the upper optical depth and lower optical depth of Kneiske et al. (2004). The parameters of the SSC model are listed in Table 2. The observed data for the HF (*open triangles*), MF (*filled triangles*), and LF (*filled circles*) are taken from Djannati-Atai et al. (1999).

In summary, the emission of the external component depends on the flare intensity, the IGMF, and the observed variation time. The flare intensity influences the flux level of the external component, and the IGMF determines the shape of the external component. It should be noted that the GeV emission of Mrk 501 was not detected by EGRET although it is a stronger TeV emitter. Our results for the case of the HF of Mrk 501 are similar to that of Dai et al. (2002); i.e., Mrk 501 is also a strong GeV emitter as long as the IGMF is weak enough.

4. DISCUSSION AND CONCLUSION

We have developed a model for possible GeV emission from a TeV blazar. In this model, photons produced both inside and

TABLE 2
PARAMETERS IN THE SSC MODEL USING THE KNEISKE ET AL. MODEL FOR THE OPTICAL DEPTH

State	δ	R (cm)	s	$\gamma_{\max}$	l_e	B (G)	$t_{\rm cross}/t_{\rm esc}$	χ^2/dof
HF	15	2×10^{16}	1.57	9×10^5	2.7×10^{-5}	0.15	1	2.1
MF	15	2×10^{16}	1.85	8×10^5	2.5×10^{-5}	0.20	1	1.9
LF	15	2×10^{16}	1.95	6×10^5	1.5×10^{-5}	0.25	1	1.2

NOTES.—The parameters in the SSC model are given by Mastichiadis & Kirk (1997) for reproducing the observed spectra in the HF, MF, and LF of Mrk 501 (Djannati-Atai et al. 1999). The model for the optical depth given by Kneiske et al. (2004) is used.

outside the source contribute to the observable GeV emission; i.e., there are two components of nonthermal photons which are responsible for the GeV emission of the source. In the source component, the photons are produced in the source through the SSC process. In the external component, the photons are produced outside the source through IC scattering of high-energy pairs produced through pair-production process of TeV photons and the IR-UV background against the CMB photons. In our model, we obtained the intrinsic spectra of a given TeV blazar by using SSC model, and then the spectra of high-energy electrons by using equation (5), which is different from the treatments of Dai et al. (2002) and Fan et al. (2004). In order to estimate the intrinsic spectrum, we used the observable spectrum (i.e., eq. [3]) predicted in the SSC model to fit the observed data in X-ray and gamma-ray energy bands for a given TeV blazar (e.g., Mrk 501), where the optical depth to high-energy photons is included. There are different models for the optical depth. In this paper, we have used two kinds, one given by Stecker et al. (2006, 2007) and one by Kneiske et al. (2004), to reproduce the observable spectra. We have applied this model to Mrk 501 to study possible GeV emission of this source during its different activities and calculated self-consistently the photon spectra of both the source and the external components. The comparison of predicted multi–wave band spectra of the source component using the two models for the optical depth with the observed data for the HF, MF, and LF of Mrk 501 are shown in Figures 3 and 7, respectively. The predicted GeV spectra for corresponding states of Mrk 501 are shown in Figures 4, 5, 6, and 8. We have shown that the properties of the GeV emission of the external component are roughly unchanged for these two models of the optical depth. The following can be seen from our calculations: (1) The flux shape of the external component depends mainly on the IGMF and becomes flatter in the lower part of this energy range as the IGMF increases, and the photons of the external component for $B_{\rm IG} \leq 10^{-20}$ G dominate over those of the source component in the energy range 100 MeV $\leq E \lesssim 100$ GeV for the HF, MF, and LF of Mrk 501, but the photons of the external component for $B_{\rm IG} = 10^{-18}$ G will be less important in the energy range $E \lesssim 1$ GeV compared to those of the source component. (2) The flux levels of the active flare states of Mrk 501 have important roles in the photon flux levels of the external component and influence the relative importance between the photon fluxes of both external and source components. (3) The photons produced in different active flares of the Mrk 501 should be detectable by *GLAST*, and if *GLAST* detects the photon emission from the Mrk 501, then the shape of photon spectrum would give the limits of the IGMF.

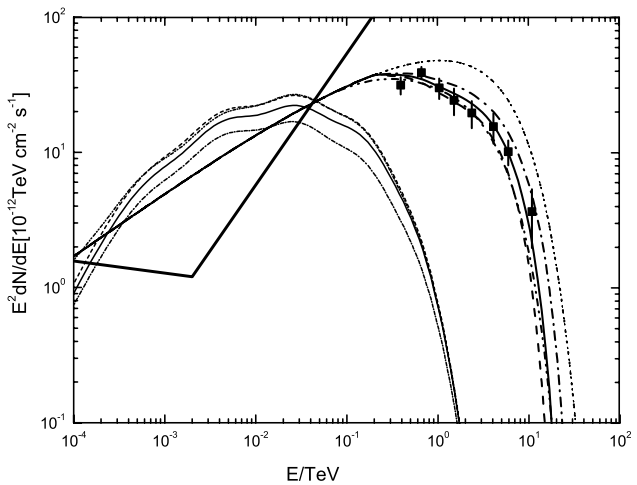

FIG. 8.—Time-averaged high-energy gamma-ray spectra of Mrk 501 for the low-intensity flare with $t_{\rm var,obs} = 0.5$ days. The dotted curves represents intrinsic spectra given by the SSC model (i.e., the spectra produced inside the source). The thick solid, dashed, dash-dotted, and dash–double-dotted curves represent the fit spectra of the average optical depth, upper optical depth, lower optical depth (Kneiske et al. 2004), and baseline model (Stecker et al. 2006), respectively. The thin curves show the secondary photon spectra produced by the resulting $e^{\pm}$ pairs interacting with CMB photons corresponding to an IGMF strength of 10^{-22} G, where the solid, dashed, dash-dotted, and dash–double-dotted curves are the same as for the thick curves. The solid squares represent the data by CAT (Djannati-Atai et al. 1999). The broken line is the *GLAST* sensitivity with integral time of 12 hr.

In this model, an important parameter is the Lorentz factor $\gamma_{e,c}$. The photons produced by high-energy electrons with $\gamma_e < \gamma_{e,c}$ contribute little to the GeV emission considered here, as pointed out by Dai et al. (2002; see also Fan et al. 2004). This Lorentz factor depends on the intergalactic magnetic field strength $B_{\rm IG}$ and the observed time variability $t_{\rm var,obs}$ (see eq. [7]). We have shown the dependence of the GeV spectrum of the external component on $B_{\rm IG}$ for a given $t_{\rm var,obs}$ and indicated that the lower part of the spectrum in the energy region from $\sim$100 MeV to $\sim$1 GeV increase as the value of $B_{\rm IG}$ decreases (e.g., see Fig. 4). On the other hand, the observed time variability also influences the shape of the GeV spectrum. We show the spectra of the external component in Figure 9, where we change the observed time variability from 0.01 to 20 days for two different values of the intergalactic magnetic field. Although the spectra are basically same for $t_{\rm var,obs} > 0.5$ days and $B_{\rm IG} = 10^{-20}$ G (see Fig. 9, *left*) and have little difference for $t_{\rm var,obs} > 0.5$ days and $B_{\rm IG} = 10^{-19}$ G (see Fig. 9, *right*), the basic property is that lower part of the spectrum for the external component is enhanced when the value of $t_{\rm var,obs}$ increases. From equation (7), $\gamma_{e,c}$ decreases as $t_{\rm var,obs}$ increases, but the value of $\gamma_{e,c}$ is limited by the pair-production process. In fact, simple argument of the pair-production condition gives $\gamma_e \gtrsim m_e c^2/2\epsilon_{\rm IR\text{-}UV}$ in order to maintain the production of the $e^{\pm}$ pairs, where $\epsilon_{\rm IR\text{-}UV}$ is the typical energy of the IR-UV background. Therefore, the lower part of the spectrum for the external component does not increase continuously with increasing $t_{\rm var,obs}$ because of the limit of the pair production to $\gamma_{e,c}$.

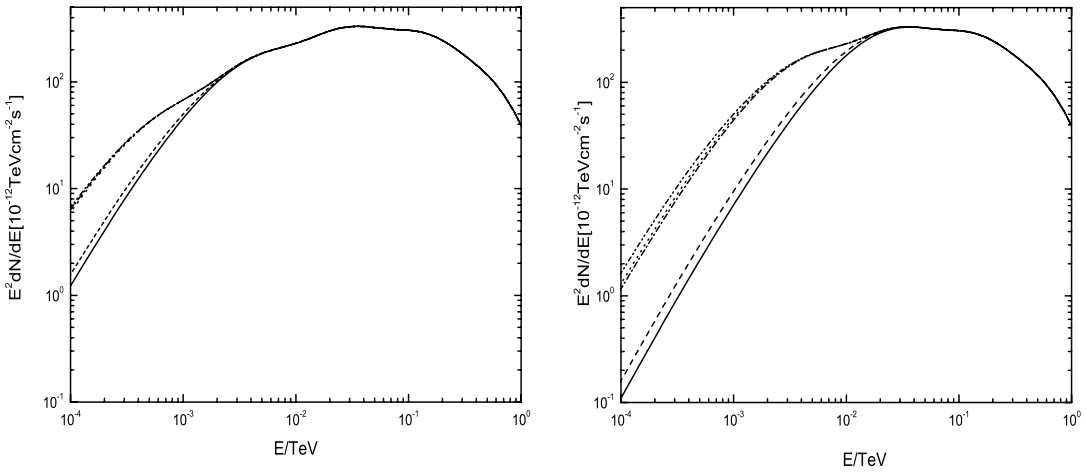

FIG. 9.—Time-averaged high-energy gamma-ray spectra of the external component in the high-intensity flare of Mrk 501 for different values of the observed variation time, $t_{\rm var,obs} = 0.01, 0.1, 0.5, 2$, and 20 days (*curves from bottom to top, respectively*). The IGMF intensity is 1×10^{-20} G in the left panel and 1×10^{-19} G in the right panel.

Finally, we would like to point out that although recent TeV observations have shown models of a high level of extragalactic background light to be inconsistent with SSC models, the low-EBL model of Kneiske et al. (2004) can explain the observed data within the frame of the SSC model. For example, Albert et al. (2007) fit the observed data of Mrk 501 in the frame of the one-zone SSC model (Tavecchio et al. 2001) using the low-EBL model of Kneiske et al. (2004). They pointed out that slightly larger energy fluxes above 1 TeV were obtained when using the EBL absorption of Stecker et al. (2006, 2007).

This work is partially supported by a Distinguished Young Scientists grant from the National Natural Science Foundation of China (NSFC 10425314), NSFC grant 10778702, and a grant from the Department of Education of Yunnan Province (07J51074).

REFERENCES

Aharonian, F. A., Timokhin, A. N., & Plyasheshnikov, A. V. 2002, A&A, 384, 834
Aharonian, F., et al. 2005, A&A, 441, 465
Albert, J., et al. 2007, ApJ, 669, 862
Blumenthal, G. R., & Gould, R. J. 1970, Rev. Mod. Phys., 42, 237
Bradbury, S. M., et al. 1997, A&A, 320, L5
Cui, W. 2007, in Italian Phys. Soc. Conf. Proc. 93, Vulcano Workshop 2006: Frontier Objects in Astrophysics and Particle Physics, ed. F. Giovannelli & G. Mannocchi (Bologna: Italian Physical Society), 207
Dai, Z. G., & Lu, T. 2002, ApJ, 580, 1013
Dai, Z. G., Zhang, B., Gou, L. J., Mészáros, P., & Waxman, E. 2002, ApJ, 580, L7
de Jager, O. C., & Stecker, F. 2002, ApJ, 566, 738
Djannati-Atai, A., et al. 1999, A&A, 350, 17
Dwek, E., & Krennrich, F. 2005, ApJ, 618, 657
Fan, Y. Z., Dai, Z. G., & Wei, D. M. 2004, A&A, 415, 483
Gliozzi, M., Sambruna, R. M., Jung, I., Krawczynski, H., Horan, D., & Tavecchio, F. 2006, ApJ, 646, 61
Gould, R., & Schréder, G. 1966, Phys. Rev. Lett., 16, 252
Hauser, M. G., & Dwek, E. 2001, ARA&A, 39, 249
Katarzynski, K., Sol, H., & Kus, A. 2001, A&A, 367, 809
Kato, T., Kusunose, M., & Takahara, F. 2006, ApJ, 638, 653
Kino, M., Takahara, F., & Kusunose, M. 2002, ApJ, 564, 97
Kneiske, T. M., Bretz, T., Mannheim, K., & Hartmann, D. H. 2004, A&A, 413, 807
Kneiske, T. M., Mannheim, K., & Hartmann, D. H. 2002, A&A, 386, 1
Konopelko, A., Mastichiadis, A., Kirk, J., de Jager, O. C., & Stecker, F. W. 2003, ApJ, 597, 851
Konopelko, A. K., Kirk, J. G., Stecker, F. W., & Mastichiadis, A. 1999, ApJ, 518, L13
Krawczynski, H. 2004, NewA Rev., 48, 367
Malkan, M. A., & Stecker, F. W. 1998, ApJ, 496, 13
———. 2001, ApJ, 555, 641
Mannheim, K. 1993, A&A, 269, 67
Mannheim, K., & Biermann, P. L. 1992, A&A, 253, L21
Maraschi, L., Ghisellini, G., & Celotti, A. 1992, ApJ, 397, L5
Mastichiadis, A., & Kirk, J. G. 1995, A&A, 295, 613
———. 1997, A&A, 320, 19
Mucke, A., & Protheroe, R. J. 2001, Astropart. Phys., 15, 121
Nikishov, A. 1962, J. Exp. Theor. Phys. Lett., 14, 393
Plaga, R. 1995, Nature, 374, 430
Primack, J. R., Bullock, J. S., Somerville, R. S., & MacMinn, D. 1999, Astropart. Phys., 11, 93
Quinn, J., et al. 1996, ApJ, 456, L83
Sigl, G., Olinto, A. V., & Jedamzik, K. 1997, Phys. Rev. D, 55, 4582
Sikora, M., Begelman, M. C., & Rees, M. J. 1994, ApJ, 421, 153
Stecker, F., & de Jager, O. C. 1998, A&A, 334, L85
Stecker, F., de Jager, O. C., & Salamon, M. H. 1992, ApJ, 390, L49
———. 1996, ApJ, 473, L75
Stecker, F., Malkan, M. A., & Scully, S. T. 2006, ApJ, 648, 774
———. 2007, ApJ, 658, 1392
Tavecchio, F., et al. 2001, ApJ, 554, 725
Wagner, R. W. 2008, MNRAS, 385, 119